

Optical-lattice-assisted magnetic phase transition in a spin-orbit-coupled Bose-Einstein condensate

Giovanni I. Martone,^{1,2,3,4,*} Tomoki Ozawa,¹ Chunlei Qu,¹ and Sandro Stringari¹

¹*INO-CNR BEC Center and Dipartimento di Fisica, Università di Trento, I-38123 Povo, Italy*

²*Dipartimento di Fisica and MECENAS, Università di Bari, I-70126 Bari, Italy*

³*INFN, Sezione di Bari, I-70126 Bari, Italy*

⁴*LPTMS, CNRS, Univ. Paris-Sud, Université Paris-Saclay, 91405 Orsay, France*

(Dated: July 9, 2018)

We investigate the effect of a periodic potential generated by a one-dimensional optical lattice on the magnetic properties of an $S = 1/2$ spin-orbit-coupled Bose gas. By increasing the lattice strength one can achieve a magnetic phase transition between a polarized and an unpolarized Bloch wave phase, characterized by a significant enhancement of the contrast of the density fringes. If the wave vector of the periodic potential is chosen close to the roton momentum, the transition could take place at very small lattice intensities, revealing the strong enhancement of the response of the system to a weak density perturbation. By solving the Gross-Pitaevskii equation in the presence of a three-dimensional trapping potential, we shed light on the possibility of observing the magnetic phase transition in currently available experimental conditions.

PACS numbers: 67.85.Bc, 67.85.Hj, 03.75.Mn, 05.30.Rt

I. INTRODUCTION

Spin-orbit-coupled Bose-Einstein condensates (BECs) are characterized by a rich variety of quantum phases, which have already been the subject of theoretical and experimental investigations (see the recent reviews [1–7] and references therein). In particular, in the case of a BEC of pseudospin $1/2$ with equal Rashba [8] and Dresselhaus [9] spin-orbit couplings, by tuning the value of the Raman coupling between the two pseudospin states one can explore different phase transitions. For relatively large values of the Raman coupling, of the order of the recoil energy, these systems exhibit a second-order transition between a plane-wave and a single-minimum phase [10, 11]. The former is characterized by the macroscopic occupation of a single-particle state with finite momentum and magnetic polarization, while in the latter the atoms populate an unpolarized state with vanishing momentum. The above transition is associated with a divergent behavior of the magnetic susceptibility and with a large increase of the effective mass. At a dynamic level it is characterized by the softening of the sound velocity [12–14] and of the frequency of the collective oscillations in the presence of harmonic trapping [15, 16]. When one decreases the value of the Raman coupling the plane-wave phase eventually disappears in favor of the so-called striped phase [11, 17–31]. In this configuration one has the appearance of periodic modulations in the density profile, whose contrast depends on the value of the Raman coupling. In the absence of an effective magnetic field the magnetic polarization vanishes in the striped phase. The phase transition between the plane-wave and the striped phases has a first-order nature. It is charac-

terized by the occurrence, on the side of the plane-wave phase, of a roton minimum in the excitation spectrum, whose energy becomes smaller and smaller as one approaches the transition [12–14, 32]. The presence of the striped phase is one of the most interesting features exhibited by spin-orbit-coupled BECs, due to its direct link to the long sought phenomenon of supersolidity [33], which takes place when two continuous symmetries (gauge and translational invariance) are spontaneously broken. So far the striped phase has not been identified directly in experiments because of the very small contrast of the density fringes in the available experimental conditions [34].

The occurrence of the roton excitation in the plane-wave phase and the emergence of the striped phase are deeply related physical phenomena. This link becomes more evident by looking at the effects of a one-dimensional static periodic potential applied to the BEC in the plane-wave phase. The linear response of the gas to a perturbation with wave vector close to the roton momentum is greatly enhanced when approaching the transition to the striped phase [12]. Beyond the linear regime, it has been shown that the application of the external potential can induce a magnetic phase transition to a fully unpolarized configuration [35]. In this paper we investigate in detail the connection between the properties of the response of the BEC at the linear and the nonlinear level. This results in a strong dependence of the behavior of the system on the parameters of the external periodic potential. For example, when its wave vector is close to the roton minimum, even a tiny static field is capable of inducing the transition to the unpolarized phase, with the appearance of highly contrasted density modulations and strong magnetic fluctuations. For wave vectors different from the roton momentum, the magnetic phase transition can take place at larger intensities of the optical lattice.

The paper is structured as follows. In Sec. II we review

* Giovanni.Martone@ba.infn.it

some relevant properties of the quantum phases of a spin-orbit-coupled BEC in uniform matter and we point out the peculiar behavior of the static density response in the plane-wave phase. Section III deals with the ground state of the system in the presence of a static optical lattice; we mainly focus on the occurrence of a magnetic phase transition, which takes place at a critical lattice intensity whose value depends in a nontrivial way on the Raman coupling and the lattice wave vector. The role of magnetic fluctuations and the effects of an external trapping potential are also investigated. We summarize in Sec. IV. Finally, in the Appendix we provide a brief description of the features of the band structure of an ideal Bose gas with spin-orbit coupling.

II. SPIN-ORBIT-COUPLED BOSE-EINSTEIN CONDENSATES IN UNIFORM MATTER

A. Single-particle Hamiltonian

The single-particle Hamiltonian first realized in the experiment of Ref. [10] reads (we set $\hbar = 1$)

$$h_0 = \frac{1}{2m} [(p_x - k_0 \sigma_z)^2 + p_\perp^2] + \frac{\Omega}{2} \sigma_x + \frac{\delta}{2} \sigma_z. \quad (1)$$

It acts on two-component spinors describing bosons with pseudospin up (\uparrow) and down (\downarrow); for simplicity, we will refer to these degrees of freedom just as the two spin states of the system. Equation (1) accounts for the presence of two counterpropagating and linearly polarized Raman lasers, which provide transitions between different hyperfine levels of the atoms, and of a bias magnetic field. The Raman coupling strength is quantified by Ω , while k_0 is the momentum transfer due to the lasers. The latter also fixes the value of the Raman recoil energy $E_r \equiv k_0^2/2m$. The linear Zeeman term δ represents an effective magnetic field, given by the sum of the Raman detuning and of the physical external magnetic field (see, for example, Ref. [12]). Finally, σ_i with $i = x, y, z$ denotes the i th Pauli matrix. For vanishing δ , when the Raman coupling Ω is smaller than $4E_r$, the lower branch of the single-particle dispersion exhibits two degenerate minima at $p_x = \pm k_1^0$, with

$$k_1^0 \equiv k_0 \sqrt{1 - \left(\frac{\Omega}{4E_r}\right)^2}, \quad (2)$$

while for $\Omega \geq 4E_r$ it has one single minimum at $p_x = 0$.

B. Many-body ground state

We now discuss the effects of the two-body interactions. In the Gross-Pitaevskii mean-field approach, the energy of an interacting system of N spin-orbit-coupled bosons

enclosed in a volume V is given by

$$E[\Psi] = \int_V d\mathbf{r} \{ \Psi^\dagger(\mathbf{r}) h_0 \Psi(\mathbf{r}) + g_1 n^2(\mathbf{r}) + g_2 s_z^2(\mathbf{r}) + g_3 n(\mathbf{r}) s_z(\mathbf{r}) \}, \quad (3)$$

where Ψ denotes the two-component condensate wave function, $n(\mathbf{r}) = \Psi^\dagger(\mathbf{r})\Psi(\mathbf{r})$ is the total density obeying the normalization condition $\int_V d\mathbf{r} n(\mathbf{r}) = N$, and $s_z(\mathbf{r}) = \Psi^\dagger(\mathbf{r})\sigma_z\Psi(\mathbf{r})$ is the longitudinal spin density. The coupling constants in Eq. (3) correspond to the combinations $g_1 \equiv (g_{\uparrow\uparrow} + g_{\downarrow\downarrow} + 2g_{\uparrow\downarrow})/8$, $g_2 \equiv (g_{\uparrow\uparrow} + g_{\downarrow\downarrow} - 2g_{\uparrow\downarrow})/8$, and $g_3 \equiv (g_{\uparrow\uparrow} - g_{\downarrow\downarrow})/4$ of the intraspecies and interspecies interaction strengths $g_{\alpha\beta}$ ($\alpha, \beta = \uparrow, \downarrow$), which are related to the corresponding s -wave scattering lengths $a_{\alpha\beta}$ via $g_{\alpha\beta} = 4\pi a_{\alpha\beta}/m$. In the following, unless otherwise specified, we will assume equal intraspecies interactions $g_{\uparrow\uparrow} = g_{\downarrow\downarrow}$, yielding $g_3 = 0$. We will also take $\delta = 0$, although the effects of a nonvanishing effective magnetic field will also be discussed qualitatively.

In the presence of antiferromagnetic spin-dependent interactions ($g_2 > 0$), when the Raman coupling Ω is small, the ground state of the many-body system corresponds to the so-called striped phase [11, 17–31]. In this configuration the density profile of the gas exhibits periodic modulations in the form of stripes, which appear as a consequence of the spontaneous breaking of translational invariance. Another relevant feature of the striped phase is the absence of magnetic polarization along z , that is, $\langle \sigma_z \rangle \equiv \int_V d\mathbf{r} s_z(\mathbf{r}) = 0$.

By increasing Ω the system enters the polarized plane-wave phase. In this phase the condensate order parameter is given by the plane-wave function $\exp(ik_1 x)$ [or $\exp(-ik_1 x)$] times a real spinor. The components of the latter have relative weights fixed by the value of the Raman coupling. The plane-wave phase is characterized by a uniform density and by a finite value $\langle \sigma_z \rangle = Nk_1/k_0$ (or $\langle \sigma_z \rangle = -Nk_1/k_0$) of the longitudinal magnetic polarization [11, 19]. The momentum k_1 in the previous formulas does not actually coincide with its single-particle value k_1^0 given by Eq. (2) because of the spin-dependent interactions proportional to g_2 ; one finds [11]

$$k_1 = k_0 \sqrt{1 - \left[\frac{\Omega}{4(E_r - \bar{n}g_2)} \right]^2}, \quad (4)$$

with $\bar{n} \equiv N/V$ the average density of the gas. To simplify the discussion, in this work we will not account for the small difference between k_1 and k_1^0 , which is negligible in the conditions of current experiments. The twofold degeneracy of the plane-wave phase highlighted above stems from a spontaneous breaking mechanism of two \mathbb{Z}_2 symmetries of the energy functional (3), similarly to what happens in usual ferromagnetic configurations. More specifically, if both δ and g_3 are vanishing, the energy (3) is invariant under the separate action of $\sigma_x \mathcal{P}$ and $\sigma_z \mathcal{T}$, with \mathcal{P} and \mathcal{T} the parity and time-reversal operator, respectively. The plane-wave phase breaks both

the above symmetries, while being invariant under their product $(\sigma_x \mathcal{P})(\sigma_z \mathcal{T})$.¹

The transition between the striped and the plane-wave phases occurs at a critical Raman coupling Ω_{tr}^0 whose value is given, in the low-density limit, by the density-independent expression [11, 19]

$$\Omega_{\text{tr}}^0 = 4E_r \sqrt{\frac{2g_2}{g_1 + 2g_2}}. \quad (5)$$

This transition is of first order and has an important magnetic character [12, 16] that has been pointed out experimentally in [10, 36]. At even larger values of the Raman coupling Ω the BEC undergoes a second-order transition to the single-minimum phase, in which the condensation momentum and the magnetic polarization are both vanishing.² We finally mention that, if the spin-dependent interactions have a ferromagnetic nature ($g_2 < 0$), only the plane-wave and the single-minimum phases appear in the phase diagram of the BEC, the striped phase being always energetically unfavored.

C. Roton excitations and compressibility

A peculiar property of the plane-wave phase is the existence of a low-energy roton minimum in the excitation spectrum, occurring at a momentum close to $2k_1$ [12–14, 32]. The energy of the roton becomes smaller and smaller as Ω approaches (from above) the critical value Ω_{tr}^0 , providing the onset of the transition to the striped phase. The roton minimum is responsible for a peculiar behavior of the static density response, i.e., the compressibility $\chi_\rho(q)$. According to the linear response theory, the compressibility can be calculated by adding, to the single-particle Hamiltonian (1), a small static periodic perturbation of the form $V_\lambda = -\lambda \rho_q + \text{H.c.}$, where $\rho_q \equiv \int_V d\mathbf{r} e^{-iqx} \hat{n}(\mathbf{r})$ and $\hat{n}(\mathbf{r})$ is the density operator. Then $\chi_\rho(q) \equiv \lim_{\lambda \rightarrow 0} \langle \rho_q \rangle_\lambda / \lambda$, where $\langle \rho_q \rangle_\lambda$ is the expectation value of ρ_q on the perturbed ground state. One finds that the function $\chi_\rho(q)$ exhibits a significant enhancement when q is close to the roton minimum [12]. A similar effect is known to characterize the static response of superfluid helium [37]. The enhancement becomes particularly strong when one approaches the phase transition to the striped phase at $\Omega = \Omega_{\text{tr}}^0$. In Fig. 1 we plot the compressibility calculated at $q = 2k_1^0$ as a function of Ω , in the presence (red solid line) and in the absence (red dotted line) of spin-orbit coupling. The values of the

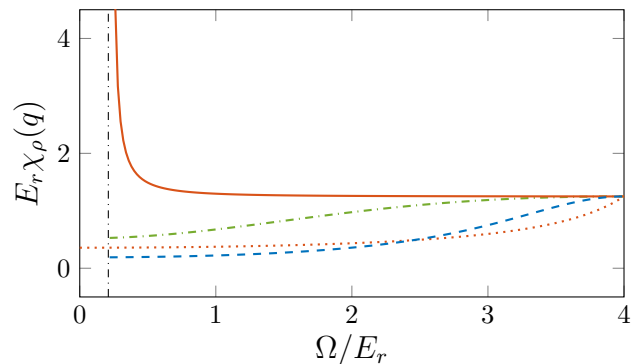


FIG. 1. (Color online) Static density response $\chi_\rho(q)$ of a spin-orbit-coupled BEC in the plane-wave phase as a function of the Raman coupling Ω , at three different values $q = 1.5k_1^0$ (green dash-dotted line), $q = 2k_1^0$ (red solid line), and $q = 3k_1^0$ (blue dashed line) of the momentum transfer. The red dotted curve corresponds to the response at $q = 2k_1^0$ of a standard Bose gas without spin-orbit coupling. The vertical black dash-dotted line identifies the critical Raman coupling Ω_{tr}^0 at which the transition to the striped phase takes place. The other parameters are $\bar{n}g_1/E_r = 0.4$ and $g_2/g_1 = 0.0012$.

average density \bar{n} and of the ratio $g_2/g_1 = 0.0012$ employed in the figure correspond to current experiments with ^{87}Rb BECs (see also the discussion in Sec. III F). In such conditions, the low-density expression (5) yields the value $\Omega_{\text{tr}}^0/E_r = 0.19$ for the critical Raman coupling, which is raised to $\Omega_{\text{tr}}^0/E_r = 0.21$ after including the small corrections due to the finite density of the system. One can notice that, for small Ω , the static response of a spin-orbit-coupled BEC at $q = 2k_1^0$ takes extremely high values as compared to those of a Bose gas without spin-orbit coupling. In the latter case the value of $\chi_\rho(q = 2k_1^0)$ for small Ω is well approximated by the asymptotic large- q behavior $\chi_\rho(q) \rightarrow 4m/q^2$. The strong enhancement of $\chi_\rho(q)$ does not take place if the momentum transfer q is significantly smaller or larger than the roton momentum; to show this, in Fig. 1 we also report the values of the compressibility in the presence of spin-orbit coupling at $q = 1.5k_1^0$ (green dash-dotted line) and $q = 3k_1^0$ (blue dashed line).

The significant dependence of the static response on the momentum transfer is reflected in the peculiar behavior of the system when entering the nonlinear regime. In particular, the large value of the compressibility close to the roton momentum suggests that nonlinear effects will emerge soon in the response, even in the presence of a tiny periodic perturbation. They are expected to give rise to highly contrasted density modulations and to important effects in the magnetic polarization of the gas, as we will discuss in the next section.

¹ Notice that the energy functional (3) keeps its invariance under $(\sigma_x \mathcal{P})(\sigma_z \mathcal{T})$ even if δ and g_3 are nonvanishing.

² This description of the phase diagram of a spin-orbit-coupled BEC with $g_2 > 0$ holds for densities \bar{n} smaller than the critical value $\bar{n}_{\text{cr}} = E_r g_1 / [2g_2(g_1 + g_2)]$. For $\bar{n} > \bar{n}_{\text{cr}}$ the plane-wave phase disappears and one has a direct first-order transition between the striped and the single-minimum phases.

III. MAGNETIC PHASE TRANSITION IN THE PRESENCE OF AN OPTICAL LATTICE

A. Variational ansatz for the ground state

Let us now explore the behavior of a spin-orbit-coupled BEC when a one-dimensional sinusoidal periodic potential of the form

$$V(\mathbf{r}) = sE_{\text{latt}} \sin^2 \frac{qx}{2} \quad (6)$$

is added to the single-particle Hamiltonian (1). In the previous expression, q denotes the momentum transferred by the two lasers, oriented along the x axis, which generate the optical lattice. The dimensionless parameter s fixes the strength of the periodic potential in units of the lattice recoil energy $E_{\text{latt}} \equiv (q/2)^2/2m$. We will focus on the case of relatively weak lattice intensities, such that the Gross-Pitaevskii mean-field description is still applicable.

There have been several studies on spin-orbit-coupled BECs in shallow optical lattices [25, 35, 38–48]. In particular, the ground state in the presence of the periodic potential (6) has been investigated in Ref. [35]. In this work we focus on the properties of a magnetic phase transition induced by the periodic potential.

First, we recall that, if the atoms condense in a state with a well-defined value of the quasimomentum k , the condensate wave function can be written in the usual Bloch form

$$\tilde{\Psi}_k(\mathbf{r}) = \sqrt{\bar{n}} e^{ikx} \sum_{\bar{K}} C_{k+\bar{K}} \begin{pmatrix} \cos \theta_{k+\bar{K}} \\ -\sin \theta_{k+\bar{K}} \end{pmatrix} e^{i\bar{K}x}. \quad (7)$$

Here \bar{K} are the reciprocal lattice vectors having values $\{\bar{m}q\}_{\bar{m} \in \mathbb{Z}}$, while $\theta_{k+\bar{K}}$ and $C_{k+\bar{K}}$ are parameters characterizing the coefficients of the Bloch wave expansion. The coefficients $C_{k+\bar{K}}$ satisfy the constraint $\sum_{\bar{K}} |C_{k+\bar{K}}|^2 = 1$, which ensures that the order parameter (7) is normalized to the total number of particles in the condensate, i.e., $\int_V d\mathbf{r} \tilde{\Psi}_k^\dagger(\mathbf{r}) \tilde{\Psi}_k(\mathbf{r}) = N$. Henceforth we will take k in the first Brillouin zone.

A good starting point for the study of the ground state of the BEC is represented by the properties of the band structure of the system in the noninteracting limit [35, 40], which are summarized in the Appendix. In particular, in the first Brillouin zone the lowest-lying energy band exhibits two degenerate minima, which occur at two opposite finite values of the quasimomentum [see Figs. 6(a) and 6(b)]. These considerations suggest that one can write an ansatz for the ground-state wave function as a superposition of two Bloch waves of the form [35]

$$\tilde{\Psi}(\mathbf{r}) = \tilde{C}_+ \tilde{\Psi}_{+k_s}(\mathbf{r}) + \tilde{C}_- \tilde{\Psi}_{-k_s}(\mathbf{r}). \quad (8)$$

Here $|\tilde{C}_+|^2 + |\tilde{C}_-|^2 = 1$ and the expressions of $\tilde{\Psi}_{\pm k_s}$ are given by Eq. (7) with $k = \pm k_s$, k_s being the magnitude of the quasimomentum in the ground state. For

an ideal Bose gas, Eq. (8) is able to reproduce the exact ground-state wave function of the system; in particular, the quasimomenta $\pm k_s$ correspond to the minima of the lowest band mentioned above, while the relative values of the coefficients \tilde{C}_+ and \tilde{C}_- remain arbitrary.

The same ansatz (8) is also well suited to study the ground state of the system in the presence of two-body interactions [35]. Before proceeding, it is worth noticing that it allows one to recover all the results presented in Sec. II for the quantum phases of the BEC in the absence of the optical lattice (i.e., for $s = 0$). In this limit the Bloch wave (7) has $C_k = 1$ and $C_{k+\bar{K}} = 0$ for $\bar{K} \neq 0$, that is, it reduces to a simple plane wave with momentum k . Consequently, the wave function (8) becomes a superposition of two counterpropagating plane waves with momenta $\pm k_s$, which coincides with the ansatz employed in the variational analysis of Ref. [11]. The plane-wave phase is reproduced by setting $k_s = k_1$, with k_1 given by Eq. (4), $\tilde{C}_+ = 1$, and $\tilde{C}_- = 0$ (or $\tilde{C}_+ = 0$ and $\tilde{C}_- = 1$ for the degenerate state with opposite momentum and magnetic polarization); if additionally k_1 vanishes, one gets instead the single-minimum phase. The striped phase corresponds to the choice $|\tilde{C}_+| = |\tilde{C}_-| = 1/\sqrt{2}$.

When the optical lattice is turned on one expects that also the plane-wave components with $\bar{K} \neq 0$ in Eq. (7) are populated. In order to study the ground state of the system at finite s , we first insert the ansatz (8) into the energy functional (3) and we deduce an expression for the energy as a function of the variational parameters k_s , $\theta_{\pm k_s + \bar{K}}$, $C_{\pm k_s + \bar{K}}$, and \tilde{C}_\pm . Then we minimize the energy at fixed values of k_0 , Ω , \bar{n} , the ratio g_2/g_1 of the interaction strengths, and the lattice parameters q and s . We have checked that the results given by this variational procedure agree with those obtained by directly solving the Gross-Pitaevskii equation in a box configuration.

B. Mixed regime

At sufficiently small values of the Raman coupling Ω , if $g_2 > 0$, the ground-state wave function of the BEC contains both the Bloch wave terms in the superposition (8) with equal weights $|\tilde{C}_+| = |\tilde{C}_-| = 1/\sqrt{2}$, giving rise to the so-called mixed phase. The properties of this phase have been studied in detail in Ref. [35]. Here we mention that it is characterized by vanishing magnetic polarization and by modulations in the density profile at two different wavelengths: The first one, equal to $2\pi/q$, is fixed by the external lattice potential, while the second one arises because of the spin-orbit coupling and is given by π/k_s . The presence of the latter entails a spontaneous breaking of the discrete translational symmetry exhibited by the energy functional (3) after the addition of the lattice potential (6). Depending on whether the two wavelengths are commensurate or not, the global oscillation of the density can be periodic or nonperiodic. The ansatz (8) actually provides only a first approximation for the wave function of the mixed phase, as it neglects the

higher-order Bloch wave terms caused by the nonlinear interactions in the energy functional (3) [22, 35]. Notice that at $s = 0$ the mixed phase smoothly connects to the striped phase, where only modulations with period π/k_s are present.

C. Unmixed regime: Magnetic phase transition

The situation becomes dramatically different if one increases Ω . Above a critical value Ω_{tr} of the Raman coupling, the mixed phase becomes energetically unfavored and a first-order transition occurs to an unmixed regime. In the latter the procedure of energy minimization yields, for the coefficients in the ansatz (8), the values $\tilde{C}_+ = 1$ and $\tilde{C}_- = 0$ or the values $\tilde{C}_+ = 0$ and $\tilde{C}_- = 1$, the two choices corresponding to the same value of the energy [35]. Hence, in the unmixed regime the wave function of the BEC is given by a single Bloch wave of the kind (7), whose quasimomentum can be assumed equal to either $+k_s$ or $-k_s$. The value of Ω_{tr} separating the mixed and unmixed configurations depends on the lattice strength s (see Fig. 3); for $s = 0$, it reduces to the critical Raman coupling Ω_{tr}^0 at which the transition from the striped to the plane-wave phase occurs [see Eq. (5) and the related discussion]. In the rest of the present paper we will focus principally on the physics of the unmixed regime, which represents the central part of our work.

The quantum phases appearing in the unmixed regime, which we discuss below, display modulations in the density profile with the same periodicity $2\pi/q$ as the external lattice potential (6). For such periodic fringes one can define the contrast as

$$I \equiv \frac{n_{\text{max}} - n_{\text{min}}}{n_{\text{max}} + n_{\text{min}}}, \quad (9)$$

where n_{max} and n_{min} are the maximum and the minimum value, respectively, taken by the density during its spatial oscillations.

For a fixed value of the Raman coupling $\Omega > \Omega_{\text{tr}}$, the properties of the ground state are determined by the competition between the density-density interaction term in the energy (3), proportional to g_1 , and the lattice potential with strength s . For very small values of s , the interactions favor a configuration where the atoms dominantly occupy the $\vec{K} = 0$ state in the superposition (7), the populations $|C_{\pm k_s + \vec{K}}|^2$ of the terms with $\vec{K} \neq 0$ being much smaller. In this phase, which smoothly connects to the plane-wave phase at $s = 0$, the ground state is twofold degenerate. In particular, the magnetic polarization $\langle \sigma_z \rangle$ is finite and takes opposite values in the two states with quasimomentum $+k_s$ and $-k_s$. As in the plane-wave phase at $s = 0$, this degeneracy stems from the spontaneous breaking of the $\sigma_x \mathcal{P}$ and $\sigma_z \mathcal{T}$ symmetries discussed in Sec. II, which are not affected by the addition of the periodic potential (6). Notice that the quasimomentum k_s approaches k_1 [see Eq. (4)] in the

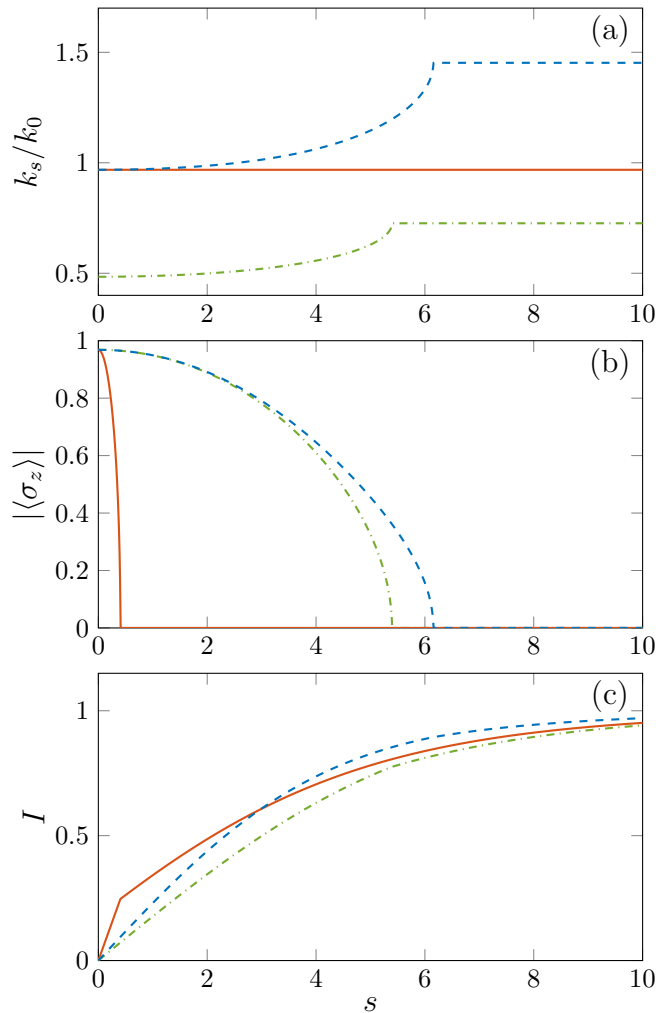


FIG. 2. (a) Condensation quasimomentum, (b) magnetic polarization, and (c) contrast of the fringes as a function of the dimensionless lattice strength s for $\Omega/E_r = 1.0$. In each panel we show the results for three different values $q = 1.5k_1^0$ (green dash-dotted line), $q = 2k_1^0$ (red solid line), and $q = 3k_1^0$ (blue dashed line) of the momentum transfer. The other parameters are $\bar{n}g_1/E_r = 0.4$ and $g_2/g_1 = 0.0012$.

limit of vanishing lattice strength, provided that k_1 belongs to the first Brillouin zone, i.e., $k_1 \leq q/2$; more in general, if the value of k_1 falls in the ℓ th Brillouin zone, then k_s tends to $|k_1 - (\ell - 1)q|$ [see, for example, the results for $q = 1.5k_1^0$ in Fig. 2(a), for which $\ell = 2$]. We will refer to the state described above as the polarized Bloch-wave phase.

As one increases s , the states with $\vec{K} \neq 0$ in Eq. (7) become more and more populated at the expense of the $\vec{K} = 0$ state. At the same time, the quasimomentum k_s , where Bose-Einstein condensation takes place, moves in the direction of the wave vector $q/2$, dictated by the optical potential [35, 40].³ This results in the decrease of

³ The last statement is true as long as the value of q is not much

the magnitude of the magnetic polarization $\langle\sigma_z\rangle$, as well as in the increase of the contrast of the fringes (9). In Fig. 2 we plot these quantities as a function of s , for a fixed value $\Omega/E_r = 1.0$ of the Raman coupling and for several choices of the lattice wave vector. In particular, for $q = 2k_1^0$ (red solid line), i.e., for a momentum transfer very close to the roton wave vector, the decrease of the magnetic polarization occurs very rapidly as one increases the optical lattice strength s . This behavior of the nonlinear response of the system to the external lattice potential (6) is deeply connected to the enhancement of the compressibility discussed in Sec. II C. Notice also that the quasimomentum k_s lies extremely close to the edge of the first Brillouin zone for any s in the $q = 2k_1^0$ case. Instead, for $q = 1.5k_1^0$ (green dash-dotted line) and $q = 3k_1^0$ (blue dashed line) the reduction of $|\langle\sigma_z\rangle|$ and the shift of k_s towards the value $q/2$ take place for larger lattice intensities.

At the critical lattice strength s_{cr} , whose value depends on Ω (see Fig. 3), the condensation quasimomentum k_s coincides with the wave vector of the periodic potential $q/2$, i.e., with the edge of the first Brillouin zone, as shown in Fig. 2(a). Since the two Bloch states having quasimomentum $\pm q/2$ are physically identical, the corresponding magnetic polarization must vanish [see Fig. 2(b)]. As a consequence, the system undergoes a second-order transition to an unpolarized Bloch wave phase. In this latter phase the populations of the various plane-wave states of Eq. (7) are balanced such that $|C_{-q/2-\bar{K}}|^2 = |C_{q/2+\bar{K}}|^2$ and $\theta_{-q/2-\bar{K}} = \pi/2 - \theta_{q/2+\bar{K}}$ for any \bar{K} ; hence, the $\sigma_x\mathcal{P}$ and the $\sigma_z\mathcal{T}$ symmetries are restored in the unpolarized state. Concerning the contrast of the density modulations (9), which we plot in Fig. 2(c), it keeps growing with s , although more slowly than in the polarized phase. Notice that in the unpolarized Bloch wave phase the contrast is much larger than the typical values exhibited in the striped phase in the absence of the lattice [34]; this is true even in the case $q = 2k_1^0$, where the magnetic phase transition, for small values of Ω [see Fig. 3(b)], takes place at extremely small values s of the optical lattice strength.

D. Phase diagram

In Fig. 3 we show the phase diagram of the system in the Ω - s plane, for the same values of the average density \bar{n} and of the interaction parameters g_1 and g_2 as the previous figures. Each panel of Fig. 3 corresponds to a different value of q [$q = 1.5k_1^0$ in Fig. 3(a), $q = 2k_1^0$ in Fig. 3(b), and $q = 3k_1^0$ in Fig. 3(c)]. In each diagram,

smaller or much larger than $2k_1^0$. In the opposite case a different behavior can take place, i.e., the condensation quasimomentum k_s moves toward the center of the Brillouin zone at $k = 0$. This effect never occurs for the values of q considered in the present work, hence we will not discuss it further.

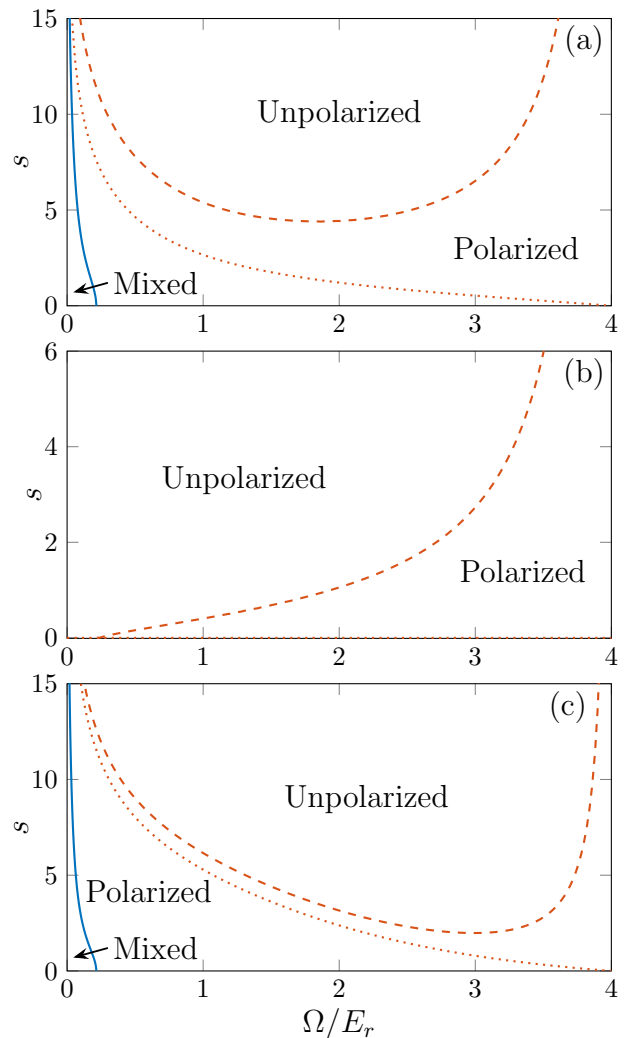


FIG. 3. (Color online) Phase diagram as a function of the Raman coupling Ω and of the dimensionless lattice strength s for (a) $q = 1.5k_1^0$, (b) $q = 2k_1^0$, and (c) $q = 3k_1^0$. The blue solid line represents the first-order transition from the mixed to the polarized Bloch wave phase. The red dashed line corresponds to the second-order transition from the polarized to the unpolarized Bloch wave phase. For the latter, the prediction of the ideal gas model is also given (red dotted lines). The other parameters are $\bar{n}g_1/E_r = 0.4$ and $g_2/g_1 = 0.0012$.

the blue solid line indicates the critical Raman coupling Ω_{tr} at which, for a given value of s , the first-order transition from the mixed to the polarized Bloch wave phase occurs. The red dashed lines show instead the behavior, as a function of Ω , of the critical lattice strength s_{cr} separating the polarized and unpolarized Bloch wave states. The predictions for s_{cr} obtained using the ideal Bose gas model (see the Appendix) are also reported (red dotted lines).

The mixed phase discussed in Sec. III B appears in a very narrow region close to the left edge of the diagrams of Figs. 3(a) and 3(c). The value of Ω_{tr} is maximum at $s = 0$, where it coincides with Ω_{tr}^0 , and becomes smaller

and smaller as the lattice intensity s increases.

The rest of the diagram is occupied by the unmixed polarized and unpolarized configurations. One can notice that, if interactions are included, the critical lattice strength s_{cr} shows a nonmonotonic behavior as a function of Ω in the $q = 1.5k_1^0$ and $q = 3k_1^0$ cases. The large values exhibited by s_{cr} at small Ω can be understood by recalling that, in this limit, the system is strongly polarized in the absence of the lattice; hence, large lattice intensities are required to achieve the transition to the unpolarized phase. In this regime of small Raman coupling the contribution of the interaction energy, being of the order of $\bar{n}g_1$ [see Eq. (3)], is less important than that of the lattice potential (6), proportional to sE_{latt} ; consequently, the interactions do not change qualitatively the behavior with respect to the prediction of the ideal Bose gas model (dotted lines). In the opposite limit of large Ω , the transition takes place at low values of s in the ideal gas model. Since $k_1^0/k_0 \ll 1$, the energy scale E_{latt} associated with the lattice potential is very small and the interactions play an important role in determining the properties of the gas. This leads to an increase of s_{cr} with respect to the values obtained within the ideal Bose gas model.

As $q \rightarrow 2k_1^0$, from both above and below, the regions of the mixed and of the unpolarized Bloch wave phases get closer and closer and eventually they touch, without the occurrence of the polarized Bloch wave phase in between. This process results in a different behavior of the phase diagram of Fig. 3(b) for $q = 2k_1^0$ with respect to those of Figs. 3(a) and 3(c). In particular, the value of s_{cr} exhibits a monotonic increasing dependence on Ω for $\Omega > \Omega_{\text{tr}}^0$. The difference with respect to the $q = 1.5k_1^0$ and $q = 3k_1^0$ cases can be better understood by taking into account that the ideal gas model, for $q = 2k_1^0$, gives rise to an unpolarized phase as soon as $s \neq 0$. The increase of s_{cr} with Ω is hence a pure effect of the two-body interactions. In Fig. 3(b) we have not included the line separating the mixed and the unpolarized Bloch wave phases; its calculation would require an accurate estimate of the energy difference between such phases, which, however, is extremely small if $q = 2k_1^0$ [this is due to the closeness of the wave vectors k_s and $q/2$ appearing in the ansatz (8) for the wave function].

It is also interesting to understand how the phase diagram discussed above depends on the density and on the interaction strengths of the BEC. For a fixed ratio g_2/g_1 , a larger density \bar{n} tends to enhance the effects of the interactions. In particular, they favor the polarized Bloch wave phase with respect to the unpolarized one, thus increasing the critical lattice strength s_{cr} for any given Ω . The same also happens for the critical Raman coupling Ω_{tr} at fixed s , which leads to the enlargement of the region of the mixed phase, in agreement with Ref. [35]. Concerning the role of the coupling constants, an increase of the ratio g_2/g_1 for a given density favors the configurations with vanishing magnetic polarization, i.e., the mixed and the unpolarized Bloch wave phases.

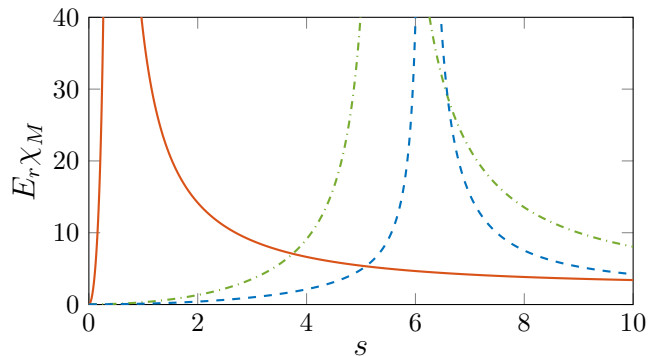


FIG. 4. Magnetic susceptibility χ_M as a function of the dimensionless lattice strength s . The parameters are the same as in Fig. 2, i.e., $\Omega/E_r = 1.0$; $q = 1.5k_1^0$ (green dash-dotted line), $q = 2k_1^0$ (red solid line), and $q = 3k_1^0$ (blue dashed line); $\bar{n}g_1/E_r = 0.4$; and $g_2/g_1 = 0.0012$.

This yields a smaller value of s_{cr} and a larger critical Raman coupling Ω_{tr} . Notice that the latter result agrees with the prediction of Eq. (5) for the $s = 0$ value of Ω_{tr} . We finally point that, unlike the mixed phase, the unpolarized Bloch wave phase can also appear in the presence of ferromagnetic spin-dependent interactions, i.e., when $g_2 < 0$.

E. Role of magnetic fluctuations

A further important signature of the magnetic phase transition occurring in our system is given by the behavior of the magnetic susceptibility χ_M . This can be evaluated in a way similar to the one described in Sec. II C for the compressibility: One adds a small perturbation $V_\lambda = -\lambda\sigma_z$ to the single-particle Hamiltonian (1) and calculates the expectation value $\langle\sigma_z\rangle_\lambda$ of the longitudinal spin operator on the perturbed ground state. Then the magnetic susceptibility is given by $\chi_M \equiv d\langle\sigma_z\rangle_\lambda/d\lambda|_{\lambda=0}$. The results show that χ_M exhibits a divergent behavior at the transition between the polarized and the unpolarized Bloch wave phases (see Fig. 4), revealing the occurrence of strong magnetic fluctuations.

Notice that, if one considers values of q too close to the roton momentum, such as $q = 2k_1^0$ (red solid line in Fig. 4), the value of the magnetic susceptibility grows very rapidly as one ramps up the lattice intensity starting from $s = 0$. Furthermore, χ_M remains large for a wide range of values of s much bigger than s_{cr} . As a consequence, the curve $\langle\sigma_z\rangle$ vs s of Fig. 2(b) and the phase diagram of Fig. 3(b) are significantly affected by the presence of a nonvanishing effective magnetic field δ or by an even tiny difference between the coupling parameters $g_{\uparrow\uparrow}$ and $g_{\downarrow\downarrow}$, as in the case of ^{87}Rb . Figure 4 also shows that the increase of the magnetic susceptibility is notably slower in the $q = 1.5k_1^0$ (green dash-dotted line) and especially in the $q = 3k_1^0$ (blue dashed line) cases. Hence, the phase diagram is much more stable if

one takes the momentum transfer q significantly different from the roton wave vector. We finally mention that the enhancement of χ_M can be further reduced by working at larger values of the Raman coupling Ω , as we do in the following section.

F. Magnetic phase transition in harmonic traps

The results discussed so far were based on a calculation in the thermodynamic limit. However, it is important to understand how they are modified if one considers a finite system in the presence of a trapping potential of harmonic type. For this purpose we have solved numerically the three-dimensional Gross-Pitaevskii equation for a gas of $N = 1.8 \times 10^5$ ^{87}Rb atoms, in the presence of an elongated trap with frequencies $(\omega_x, \omega_y, \omega_z) = 2\pi \times (50, 50, 140)$ Hz. The scattering lengths are $a_{\uparrow\uparrow} = 100.83a_B$ and $a_{\downarrow\downarrow} = a_{\uparrow\downarrow} = 100.37a_B$, a_B being the Bohr radius. The value of the momentum transfer due to the Raman laser is set to $k_0 = 5.52 \mu\text{m}^{-1}$. All the above parameters correspond to the conditions of the experiment of Ref. [10]. For this calculation we have taken the Raman coupling $\Omega/E_r = 3.0$ and the momentum transfer $q = 3k_1^0 = 1.98k_0$. This choice corresponds to working close to the minimum of the critical lattice intensity s_{cr} appearing in Fig. 3(c); furthermore, following the discussion in Sec. III E, one can expect that magnetic fluctuations will be less important in this regime of the parameters.

In Fig. 5 we report our predictions (blue squares) for the quasimomentum [Fig. 5(a)], the magnetic polarization [Fig. 5(b)], and the contrast of the fringes in the integrated density $n_1(x) = \int dy dz n(\mathbf{r})$ close to the center of the sample [Fig. 5(c)]. Notice that, since $g_3 > 0$ for the above values of the scattering lengths, the quasimomentum and the magnetic polarization must actually be negative; in the figure we only plot their magnitudes. Our results clearly show that the emergence of the magnetic phase transition can be detected also in trapped configurations. Furthermore, we have checked that, at variance with the choice of small Ω and of q too close to the roton momentum, the results of the simulations are not significantly perturbed by the inclusion of a small but finite effective magnetic field δ .

Also in Fig. 5 we also report the results (blue dashed lines) for an infinite system whose average density \bar{n} coincides with the density at the center of the trapped BEC described above. By comparing the two sets of data, one immediately sees that the results for the two systems are slightly different from the quantitative point of view. Indeed, as a consequence of the spatially varying density, the values of the magnetic polarization in the trapped gas are smaller than in the infinite system and they decrease more rapidly with increasing s . However, the qualitative behavior is very similar to the one in the absence of the trap.

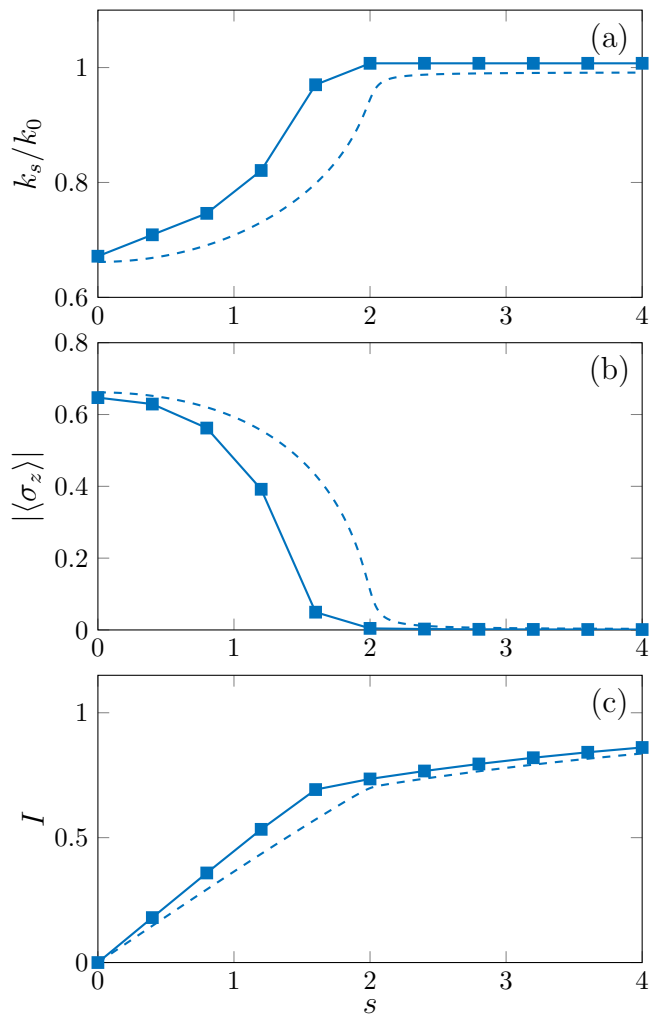


FIG. 5. (a) Condensation quasimomentum, (b) magnetic polarization, and (c) contrast of the fringes as a function of the dimensionless lattice strength s for $\Omega/E_r = 3.0$ and $q = 3k_1^0 = 1.98k_0$. The dashed line corresponds to the case of an infinite system with $\bar{n}g_1/E_r = 0.4$, $g_2/g_1 = 0.0012$, and $g_3/g_2 = 2.0$. The squares are the results for a three-dimensional trapped gas in the conditions described in the text, which yield a density at the center of the trap equal to the average density \bar{n} of the infinite system.

IV. CONCLUSION

The static response to a weak density perturbation of a spin-orbit-coupled Bose-Einstein condensate in the plane-wave phase exhibits an important dependence on the wave vector of the external potential. If the latter is close to the momentum at which the roton minimum occurs, the response acquires a very large value close to the transition to the striped phase. This phenomenon is related to the vanishing of the energy of the roton minimum and reveals the presence of important highly non-linear effects. By studying the ground state of the system in the presence of a one-dimensional optical lattice, we have shown that such effects are strongly connected

with the occurrence of a second-order magnetic phase transition to an unpolarized Bloch wave phase. In this state the contrast of the density modulations can achieve much larger values than in the striped phase appearing at low Raman couplings in the absence of the lattice. The critical lattice intensity needed to achieve the magnetic phase transition can assume very tiny values if the lattice wave vector is close to the roton momentum; in the opposite case, the transition can take place at larger lattice strengths. The phase transition is accompanied by a divergent behavior of the magnetic susceptibility. The stability of the system against magnetic fluctuations can be enhanced by choosing the momentum transfer due to the optical lattice far enough from the roton momentum and considering large values of the Raman coupling. Our predictions for infinite systems have been confirmed also by Gross-Pitaevskii calculations in a three-dimensional trap with realistic parameters, which opens the possibility of exploring these nonlinear phenomena in current experiments.

ACKNOWLEDGMENTS

Useful correspondence and discussions with Peter Engels, Amin Khamenechi, and Yun Li are acknowledged. G.I.M. was partially supported by the PRIN Grant No. 2010LLKJBX “Collective quantum phenomena: From strongly correlated systems to quantum simulators” and by INFN through the project “QUANTUM.” The research leading to these results received funding from the European Research Council under European Community’s Seventh Framework Programme (FR7/2007-2013 Grant Agreement No. 341197). T.O., C.Q., and S.S. were supported by ERC through the QGBE grant, by the QUIC grant of the Horizon2020 FET program, and by Provincia Autonoma di Trento. T.O. was also supported by the EU-FET Proactive grant AQUUS, Project No. 640800.

Appendix: Band structure of the ideal Bose gas

As discussed in Sec. II B, in the absence of the periodic potential (6) and for $\Omega > \Omega_{tr}^0$, the minima of the energy (3) of a spin-orbit-coupled BEC occur at two momenta $\pm k_1$, with k_1 given by Eq. (4). In Sec. III C it was pointed out that, by increasing the intensity s of the periodic potential, one forces the system to adapt its minima to become closer to the wave vector $q/2$ of the external periodic potential. Eventually, when the separation be-

tween the two minima equals q , i.e., when the two minima coincide with the edges of the Brillouin zone, they correspond to the same physical state. As a consequence, the magnetic polarization disappears.

The above mechanism is simply understood in the ideal Bose gas model described by the spin-orbit Hamiltonian (1) with the addition of the lattice potential (6) [40].

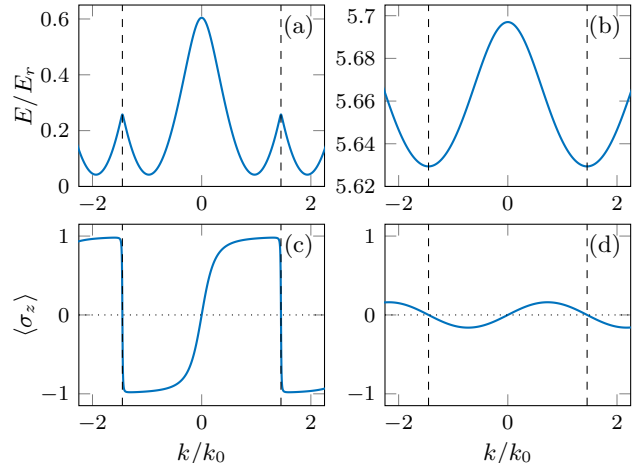


FIG. 6. (a) and (b) Lowest-lying energy band of the single-particle dispersion of a spin-orbit-coupled BEC in a one-dimensional optical lattice and (c) and (d) the corresponding magnetic polarization as a function of the quasimomentum k , for $\Omega/E_r = 1.0$ and $q = 3k_1^0 = 2.9k_0$. The left and right panels show the results for $s = 0.1$ and $s = 10.0$, respectively. The region between the vertical dashed lines corresponds to the first Brillouin zone.

In Fig. 6 we show the lowest-lying band of the single-particle dispersion for $\Omega/E_r = 1.0$, $q = 3k_1^0 = 2.9k_0$, and two different values of s . If s is small, the distance of the two minima at $k = \pm k_s$ significantly differs from q and they carry opposite magnetic polarizations given by $\sim \pm k_s/k_0$, as shown in Figs. 6(a) and 6(c), respectively. By increasing the value of s the two minima eventually approach the edge of the Brillouin zone and the polarization disappears [see Figs. 6(b) and 6(d)]. Although these examples refer to a situation with $q > 2k_1^0$, a similar behavior can take place in the opposite case of $q < 2k_1^0$, i.e., when the value of k_1^0 does not lie in the first Brillouin zone (see the discussion in Sec. III C).

Finally, it is worth noting that, if one chooses $q = 2k_1^0$, the single-particle dispersion minima are located at the edge of the Brillouin zone for any nonvanishing value of s . Thus, the ground state in the ideal Bose gas model is unpolarized as soon as $s \neq 0$.

-
- [1] J. Dalibard, F. Gerbier, G. Juzeliūnas, and P. Öhberg, Rev. Mod. Phys. **83**, 1523 (2011).
 [2] V. Galitski and I. B. Spielman, Nature (London) **494**, 49

- (2013).
 [3] X. Zhou, Y. Li, Z. Cai, and C. Wu, J. Phys. B **46**, 134001 (2013).

- [4] N. Goldman, G. Juzeliūnas, P. Öhberg, and I. B. Spielman, *Rep. Prog. Phys.* **77**, 126401 (2014).
- [5] H. Zhai, *Rep. Prog. Phys.* **78**, 026001 (2015).
- [6] Y. Li, G. I. Martone, and S. Stringari, in *Annual Review of Cold Atoms and Molecules*, edited by K. W. Madison, K. Bongs, L. D. Carr, A. M. Rey, and H. Zhai (World Scientific, Singapore, 2015), Chap. 5, Vol. 3, pp. 201–250.
- [7] Y. Zhang, M. E. Mossman, T. Busch, P. Engels, and C. Zhang, *Front. Phys.* **11**, 118103 (2016).
- [8] Y. A. Bychkov and E. I. Rashba, *J. Phys. C* **17**, 6039 (1984).
- [9] G. Dresselhaus, *Phys. Rev.* **100**, 580 (1955).
- [10] Y.-J. Lin, K. Jimenez-Garcia, and I. B. Spielman, *Nature (London)* **471**, 83 (2011).
- [11] Y. Li, L. P. Pitaevskii, and S. Stringari, *Phys. Rev. Lett.* **108**, 225301 (2012).
- [12] G. I. Martone, Y. Li, L. P. Pitaevskii, and S. Stringari, *Phys. Rev. A* **86**, 063621 (2012).
- [13] W. Zheng, Z.-Q. Yu, X. Cui, and H. Zhai, *J. Phys. B* **46**, 134007 (2013).
- [14] S.-C. Ji, L. Zhang, X.-T. Xu, Z. Wu, Y. Deng, S. Chen, and J.-W. Pan, *Phys. Rev. Lett.* **114**, 105301 (2015).
- [15] J.-Y. Zhang, S.-C. Ji, Z. Chen, L. Zhang, Z.-D. Du, B. Yan, G.-S. Pan, B. Zhao, Y.-J. Deng, H. Zhai, S. Chen, and J.-W. Pan, *Phys. Rev. Lett.* **109**, 115301 (2012).
- [16] Y. Li, G. I. Martone, and S. Stringari, *EPL* **99**, 56008 (2012).
- [17] C. Wang, C. Gao, C.-M. Jian, and H. Zhai, *Phys. Rev. Lett.* **105**, 160403 (2010).
- [18] C.-J. Wu, I. Mondragon-Shem, and X.-F. Zhou, *Chin. Phys. Lett.* **28**, 097102 (2011).
- [19] T.-L. Ho and S. Zhang, *Phys. Rev. Lett.* **107**, 150403 (2011).
- [20] S. Sinha, R. Nath, and L. Santos, *Phys. Rev. Lett.* **107**, 270401 (2011).
- [21] T. Ozawa and G. Baym, *Phys. Rev. A* **85**, 063623 (2012).
- [22] Y. Li, G. I. Martone, L. P. Pitaevskii, and S. Stringari, *Phys. Rev. Lett.* **110**, 235302 (2013).
- [23] D. A. Zezyulin, R. Driben, V. V. Konotop, and B. A. Malomed, *Phys. Rev. A* **88**, 013607 (2013).
- [24] Z. Lan and P. Öhberg, *Phys. Rev. A* **89**, 023630 (2014).
- [25] W. Han, G. Juzeliūnas, W. Zhang, and W.-M. Liu, *Phys. Rev. A* **91**, 013607 (2015).
- [26] S. S. Natu, X. Li, and W. S. Cole, *Phys. Rev. A* **91**, 023608 (2015).
- [27] Q. Sun, L. Wen, W.-M. Liu, G. Juzeliūnas, and A.-C. Ji, *Phys. Rev. A* **91**, 033619 (2015).
- [28] R. Liao, O. Fialko, J. Brand, and U. Zülicke, *Phys. Rev. A* **92**, 043633 (2015).
- [29] K. Sun, C. Qu, Y. Xu, Y. Zhang, and C. Zhang, *Phys. Rev. A* **93**, 023615 (2016).
- [30] Z.-Q. Yu, *Phys. Rev. A* **93**, 033648 (2016).
- [31] G. I. Martone, F. V. Pepe, P. Facchi, S. Pascazio, and S. Stringari, *Phys. Rev. Lett.* **117**, 125301 (2016).
- [32] M. A. Khamehchi, Y. Zhang, C. Hamner, T. Busch, and P. Engels, *Phys. Rev. A* **90**, 063624 (2014).
- [33] M. Boninsegni and N. V. Prokof'ev, *Rev. Mod. Phys.* **84**, 759 (2012).
- [34] G. I. Martone, Y. Li, and S. Stringari, *Phys. Rev. A* **90**, 041604 (2014).
- [35] Z. Chen and Z. Liang, *Phys. Rev. A* **93**, 013601 (2016).
- [36] S.-C. Ji, J.-Y. Zhang, L. Zhang, Z.-D. Du, W. Zheng, Y.-J. Deng, H. Zhai, S. Chen, and J.-W. Pan, *Nat. Phys.* **10**, 314 (2014).
- [37] F. Dalfovo and S. Stringari, *Phys. Rev. B* **46**, 13991 (1992).
- [38] J. Larson, J.-P. Martikainen, A. Collin, and E. Sjöqvist, *Phys. Rev. A* **82**, 043620 (2010).
- [39] H. Sakaguchi and B. Li, *Phys. Rev. A* **87**, 015602 (2013).
- [40] Y. Zhang and C. Zhang, *Phys. Rev. A* **87**, 023611 (2013).
- [41] Y. V. Kartashov, V. V. Konotop, and F. K. Abdullaev, *Phys. Rev. Lett.* **111**, 060402 (2013).
- [42] Y. Cheng, G. Tang, and S. K. Adhikari, *Phys. Rev. A* **89**, 063602 (2014).
- [43] M. Salerno and F. K. Abdullaev, arXiv:1501.07296.
- [44] C. Hamner, Y. Zhang, M. A. Khamehchi, M. J. Davis, and P. Engels, *Phys. Rev. Lett.* **114**, 070401 (2015).
- [45] W. Li, L. Chen, Z. Chen, Y. Hu, Z. Zhang, and Z. Liang, *Phys. Rev. A* **91**, 023629 (2015).
- [46] Y. Zhang, Y. Xu, and T. Busch, *Phys. Rev. A* **91**, 043629 (2015).
- [47] T. F. J. Poon and X.-J. Liu, *Phys. Rev. A* **93**, 063420 (2016).
- [48] H. M. Hurst, J. H. Wilson, J. H. Pixley, I. B. Spielman, and S. S. Natu, arXiv:1608.01346.